# Dynamics and structural features of the microtubule plus-ends in interphase mouse fibroblasts

Zovko, S.

CHAPTER III

# Microtubule plus-end conformations and dynamics in the periphery of interphase mouse fibroblasts

Sandra Zovko, Jan Pieter Abrahams, Abraham J. Koster , Niels Galjart and A. Mieke Mommaas

*Mol. Biol. Cell 19, 3138-3146.*

## Microtubule plus-end conformations and dynamics in the periphery of interphase mouse fibroblasts

*The plus-ends of microtubules (MTs) alternate between phases of growth, pause and shrinkage - a process called "dynamic instability". Cryo-EM of in vitro assembled MTs indicates that the dynamic state of the plus-end corresponds with a particular MT plus-end conformation. Frayed ("ram's horn like"), blunt and sheet conformations are associated with shrinking, pausing and elongating plus-ends, respectively. A number of new conformations have recently been found in situ but their dynamic states remained to be confirmed. Here, we investigated the dynamics of MT plus-ends in the peripheral area of interphase mouse fibroblasts (3T3s) using electron microscopical and tomographical analysis of cryo-fixed, freeze-substituted and flat-embedded sections. We identified nine morphologically distinct plus-end conformations. The frequency of these conformations correlates with their proximity to the cell border, indicating that the dynamic status of a plus-end is influenced by features present in the periphery.*

*Shifting dynamic instability towards depolymerization with nocodazole enabled us to address the dynamic status of these conformations. We suggest a new transition path from growth to shrinkage via the so-called sheet-frayed and flared ends and we present a kinetic model that describes the chronology of events taking place in nocodazole-induced MT depolymerization.*

## Introduction

The microtubule (MT) network forms a major component of the cytoskeleton of the eukaryotic cell. MTs are involved in a number of vital cellular processes, including cell division, cell motility, general cell morphology and cargo transport. MTs are hollow ~25 nm diameter tubes assembled from α/β-tubulin heterodimers, which are organized in a head-to-tail fashion in protofilaments that laterally interact with each other (Mandelkow and Mandelkow, 1985). The plus-end, exposing the β-tubulin subunits, is dynamically unstable and oscillates between phases of relatively slow growth, pausing and rapid shrinkage. The switch from growth to shrinkage is termed “catastrophe” and the switch from shrinkage to growth “rescue”. The minus-end, exposing the α-tubulin subunits, is less dynamic (Mitchison and Kirschner, 1984; Mitchison, 1993). In many cell types the MT minus-end is embedded in the MT organizing centre, or MTOC.

Both tubulin subunits bind GTP (Caplow and Reid, 1985) but only the β-subunit hydrolyzes GTP. MTs elongate by the addition of GTP-bound tubulin subunits or small oligomers at the MT plus-end (Kerssemakers *et al.,* 2006). Longitudinal contacts within the MT lattice stimulate the β-subunits of polymerized tubulin to hydrolyze GTP. The crucial feature behind dynamic instability is thought to be the difference in structure between the GTP-tubulin heterodimer and GDP-tubulin heterodimer: the first is relatively straight, while the GDP-tubulin heterodimer exhibits a curved conformation (Caplow *et al.,* 1992b; Ravelli *et al.,* 2004; Krebs *et al.,* 2005; Nogales and Wang, 2006). As the GDP-dimers in the protofilaments of the MT are forced to stay straight by lateral contacts, the energy of the curvature is stored within the lattice in the form of tension, making MTs unstable and easy to depolymerize (Caplow *et al*., 1994b) .When the GTP-cap at the end of a MT is lost, protofilaments can adopt a curved conformation, resulting in the weakening of lateral interactions between the protofilaments, and causing a catastrophe and collapse of the the MT (Caplow *et al.,* 1994b; Janosi *et al*., 2002; Nogales and Wang, 2006).

Cryo-electron microscopy (cryo-EM) studies of *in vitro* assembled or extracted MTs indicated that the phases of shrinkage, pausing and growth might correspond to specific structures at the plus-end. These are called *frayed* (*coiled, “ram’s horn”*), *blunt* and *extended* (*straight, tapered, sheet-like*), respectively (Mandelkow, 1991; Chrétien *et al*., 1995; Arnal *et al*., 2000). In the elongation phase, as the GTP-tubulin dimers and/or small oligomers are added at the plus-end, a two dimensional sheet is formed, which gradually closes in a zipper-like fashion (Chrétien *et al*., 1995; Kerssemakers *et al*., 2006; Wang and Nogales, 2005; Nogales and Wang, 2006). The sheet can close to form a tube thereby adopting the *blunt* end conformation (Chrétien *et al.,* 1995; Arnal *et al.,* 2000), which was suggested to be a metastable transition state between growth and shrinkage (Tran *et al.,* 1997; Arnal *et al*., 2000; Janosi *et al*., 2002). Loss of the GTP-cap triggers curving of the protofilaments (i.e. GTP-tubulin becomes GDP-tubulin which has a relatively curved conformation), which then peel off outwards from the MT axis (*frayed* end).

Insight in MT dynamic instability and the factors influencing it *in vivo* is essential for understanding the nature of malfunction of MT dynamics in diseased cells. *In vivo*, MT dynamics is regulated by a variety of cellular factors (Lieuvin *et al*., 1994; Saoudi *et al*., 1998; Perez *et al*., 1999; Schuyler *et al*., 2001; Kovacs and Csaba, 2005; Lansbergen and Akhmanova, 2006). Furthermore, MTs *in vivo* predominantly have 13 protofilaments,

whereas MTs assembled *in vitro* are made of either 13 or 14 protofilaments. These structural differences seem to be reflected by the plus-end of MTs *in vivo.* In recent years, studies of kinetochore MT (kMT) plus-ends in *C. elegans* (O'Toole *et al.*, 2003), plant cells (Austin *et al.,* 2005), $PtK_1$ and *Drosophila* cells (VandenBeldt *et al.* 2006; Maiato *et al.*, 2006) and in yeast (Höög *et al.*, 2007) not only confirmed the existence of the plus-end conformations observed *in vitro* but also introduced a number of new conformations. Not all of the newly introduced forms were found in each of these studies and their dynamic states remained unknown.
To gain more insight into MT dynamic instability *in vivo*, we studied MT plus-ends of interphase mouse 3T3 fibroblasts using EM, electron tomography (ET) and fluorescence microscopy. We focused on MT plus-ends in the very periphery of these cells, for it is known that dynamic instability is enhanced at the cell membrane (Komarova *et al*., 2002; Vorobjev *et al*., 2003). In order to correlate a particular MT plus-end conformation to its dynamic state, we studied depolymerization kinetics using nocodazole. Furthermore, we quantified the distribution of plus-end conformations over two zones within the cell periphery. On the basis of our results, we propose a kinetic model which integrates the dynamic state of MT plus-ends with their conformation.

## Material and Methods

### *Cell culture*

Mouse 3T3 fibroblasts were cultured in DMEM, supplemented with 10% fetal bovine serum, 2mM L-Glutamine and antibiotics, in a humidified atmosphere with 5% $CO_2$ at 37°C.

### *Specimen preparation for electron microscopy*

3T3 cells were grown on 13mm diameter Thermanox™ (NUNC) coverslips for two days (70% confluence). The cells were cryo-fixed by plunge-freezing the coverslips in liquid ethane in an automated system with a temperature and humidity controlled chamber. The atmosphere in the chamber was humid and had a temperature of 37°C. It took 10 seconds between putting the coverslip with cells into the chamber and plunging it, while vitrification was instantaneous upon plunging.
Cryo-immobilized samples were then subjected to freeze-substitution in a mixture of 0.01% OsO4 and 0.25% uranyl acetate in absolute acetone. Freeze-substitution was performed in Automatic Freeze Substitution apparatus (AFS, Leica) for 72 hours at -90°C. The temperature was then gradually raised (10°/h) to -20°C and maintained at this temperature for 12 hours. Afterwards, the temperature was raised to 0°C (10°/h).
Subsequently, cells were washed twice for 15 minutes with acetone. The specimens were then infiltrated with epoxy resin and flat-embedded. Sections of 100-150 nm were made parallel to the cell attachment plane. The samples were post-stained with uranyl acetate and lead-salt mixture for 15 and 5 minutes respectively.

### *Electron microscopy and electron tomography*

Thin sections were analyzed using a CM-10 Transmission Electron Microscope with a LaB6 filament operating at 80kV.

For quantitative analysis, various plus-ends in the area of maximally 5 µm from the plasma membrane towards the cell interior were scored and categorized. In total 164 plus-ends were scored. Projection of a MT shows two dark lines caused by the superposition of protofilaments in the direction of projection (i.e. the 'sides' of the MT), having a higher signal than the 'bottom' and 'top' of the MT. Classification was based on the degree of line curvature and on the difference in line length at the plus-end of the MT. False positives (MT cut gratingly) were filtered out.

3D tomograms were collected on previously classified MT plus-ends in order to verify the classification based on 2D images. Using Inspect 3D (FEI Company) software, tomographic series of MT plus-ends were collected performing single-axis tilt series from –60 to +60 degrees with increments of 1° in a Tecnai-12 (FEI) equipped with a LaB6 filament operating at 120 kV. 2kx2k binned images were recorded in focus using a CCD camera (4k Eagle) at a magnification of 30 000x. Tomographic tilt series were analyzed and processed using IMOD (Colorado University, Boulder). Projection images were preprocessed by hot pixel removal and roughly aligned by cross-correlation. Final alignment was performed using 10nm colloidal gold as fiducial markers (Ress *et al*., 1999). Tomograms were obtained using weighted back-projection.

To establish the potential correlation between plus-end conformations and their location within the cell, the cell periphery was divided into two zones, either 0-2 µm or 2-5 µm away from the cell border. In zone 0-2 µm 51 MT plus-ends and in the zone 2-5 µm 113 MT plus-ends could be classified.

### *Kinetic analysis of MT depolymerization by nocodazole in 3T3 cells*

For the MT shrinkage-induction experiments cells were exposed to 10µM nocodazole (dissolved in culture medium) for 5, 30, 60 or 120 seconds prior to blotting and subsequent freezing. Since there is a 10s delay between blotting and vitrification (which stops depolymerization), the total exposure times to nocodazole were 15, 40, 70 and 130s, respectively. The experiment was replicated three times for each time point. During the exposure to nocodazole, the cells were kept at 37°C in a humidified atmosphere with 5% $CO_2$. Cryo-fixation and freeze-substitution followed by flat embedding were performed as described above.

We analyzed 451 MT plus-ends in nocodazole-treated cells in total using electron microscopy as described above.

For the analysis of the nocodazole time series, the frequency distribution of plus-end states of unexposed cells was used as the starting situation at (t = 0s). At every time point, mean percentages of the various conformations of plus-ends (together with their standard deviations[1]) were calculated from these triplicates. Two conformations (*sheet-straight* and *sheet-frayed 1*), were not observed at t=130s, and at these two points the standard deviation was assumed to be equal to √⅔ times the expected frequency.

[1] $\sigma_t = \sqrt{((\Sigma(f_{o,t}-f_{m,t})^2)/(N-1))}$

Where: $\sigma_t$ is the standard deviation at time t, $f_{o,t}$ is the observed frequency at time t, $f_{m,t}$ is the mean frequency at time t, N is 3 (every experiment was performed in triplicate).

### *Scoring plus-ends by fluorescence microscopy*

3T3 fibroblasts were grown overnight to ~40% of confluence on glass coverslips, prior to cryo-fixation (see above) and freeze-substitution in pure acetone without additional fixatives. When a temperature of -20°C was reached, samples were fixed with methanol/EGTA for 12 minutes. Subsequently, cells were washed with PBS and incubated in blocking buffer for 45 minutes at room temperature. Cells were incubated for one hour at room temperature with primary antibodies against tyrosinated tubulin (rat monoclonal, clone YL1/2, Abcam), diluted in blocking buffer, and against a marker of the plus-ends of growing MTs (EB1, mouse monoclonal, Transduction laboratories), diluted in blocking buffer. The samples were washed three times for 15 minutes in PBS/0.05% Tween-20 and incubated with goat-anti-rat-Alexa488 and goat-anti-mouse-Alexa594 secondary antibody (both Molecular Probes) for one hour at RT. Next, cells were washed three times in PBS/0.05% Tween-20, and in 70% and 100% ethanol, air dried and mounted on a glass slide using Vectashield mounting medium with DAPI nuclear staining.

Immuno-fluorescent images were collected using a Leica DMRXA microscope with a Coolsnap K4 camera using ColorPro software. MT plus-ends, stained for EB1 or tubulin, were scored in the cytoplasm up to ~5µm from the cell border. Only areas of the cell where MTs were sparse enough to distinguish them separately were used for analysis.

The fluorescence microscopy images were processed with Photoshop (Adobe). The area of interest (~5 µm from the cell border inwards) was marked. To improve visibility of the MT contrast, an emboss filter was applied (0 and 90 degrees). Next, the MTs were manually tracked and marked at both 0 and 90 degrees emboss images in two different colors. The two images were then superimposed, resulting in good visibility of the MTs in the images. The superimposed image revealed the spatial position of the MTs in the cell periphery, enabling scoring of the total number of MTs and MT plus-ends.

## Results

### *Nine distinct plus-end conformations in the periphery of interphase 3T3 cells*

In order to produce a sample in which we could trace MTs, and therefore reliably locate MT plus-ends, several experimental procedures were introduced. First, we used Thermanox® coverslips instead of glass, since the latter break upon Epon capsule removal. 3T3 cells grown on Thermanox® coverslips were flat and spread out properly allowing easy cryo-vitrification of the sample. Flat-embedded cells could then be sectioned in the plane of cell attachment, ensuring sample sections largely parallel to the MT-network. As 3T3 cells have a relatively large and flat periphery, the MT network could be studied in a single thin plane, often 200-100 nm thick (Figure 1A).

We selected and categorized MT-ends which pointed towards the cell membrane, since these are predominantly MT plus-ends rather than minus-ends (Figure 1B and Figure 1C). Electron tomography enabled us to extract 3D representations of the plus-ends inside the tomographic volume. This allowed further 3D characterization of the various plus-end features and permitted relating these to their projection images.

Taking distinct morphological characteristics of MT plus-ends into account (see *Material and Methods* and Wade and Chrétien, 1993) we were able to classify them into nine groups. Example projection images and tomographic slices of the nine MT plus-end

conformations are shown in Figure 1, D-F. The *early-frayed* and *frayed* ends are characterized by the ram's horns conformation (Mandelkow and Mandelkow, 1985), *i.e.* the protofilaments at both sides of the MT end curve away to a similar extent from the MT axis. The *early-frayed* end is characterized by relatively short tips of protofilaments bending away from the MT axis (VandenBeldt *et al.*, 2006) while in the *frayed* end protofilaments curve away further, resulting in protofilament coils. The degree of projected protofilament curvature was defined as the angle between the MT wall and the straight line drawn from the point the bending started to the tip of the curved protofilament. In the *early-frayed* end this angle ranged from 19° to 45° with an average angle of 35° ± 10°. In the *frayed* end the curvature angle ranged from 54° to 180° with average angle of 106° ± 31°.

MT-ends of the *forked* conformation are directed away from the MT axis, but they are straight rather than curved. In projection, this outward redirection of straight protofilaments appears to introduce a "break", or "kink" in the MT lattice. The protofilaments in the *forked* end terminate more or less simultaneously. By contrast, in the *sheet-frayed 2* end we observed the protofilaments to curve away from the MT axis at different heights. In the *sheet-frayed 2* plus-end, the curvature of protofilaments pointing away from the lattice was similar to that of the *early-frayed* and *frayed* ends.

The *sheet-straight* conformation has straight ends of unequal length. Thus, the straight-sheet resembles sheet-frayed 2 except that the latter has curving protofilaments, as in (*early)-frayed* plus-ends. The sheet length (distance between the protofilament ends at the "long" and "short" sides of the lattice) was found to range from 50-320 nm

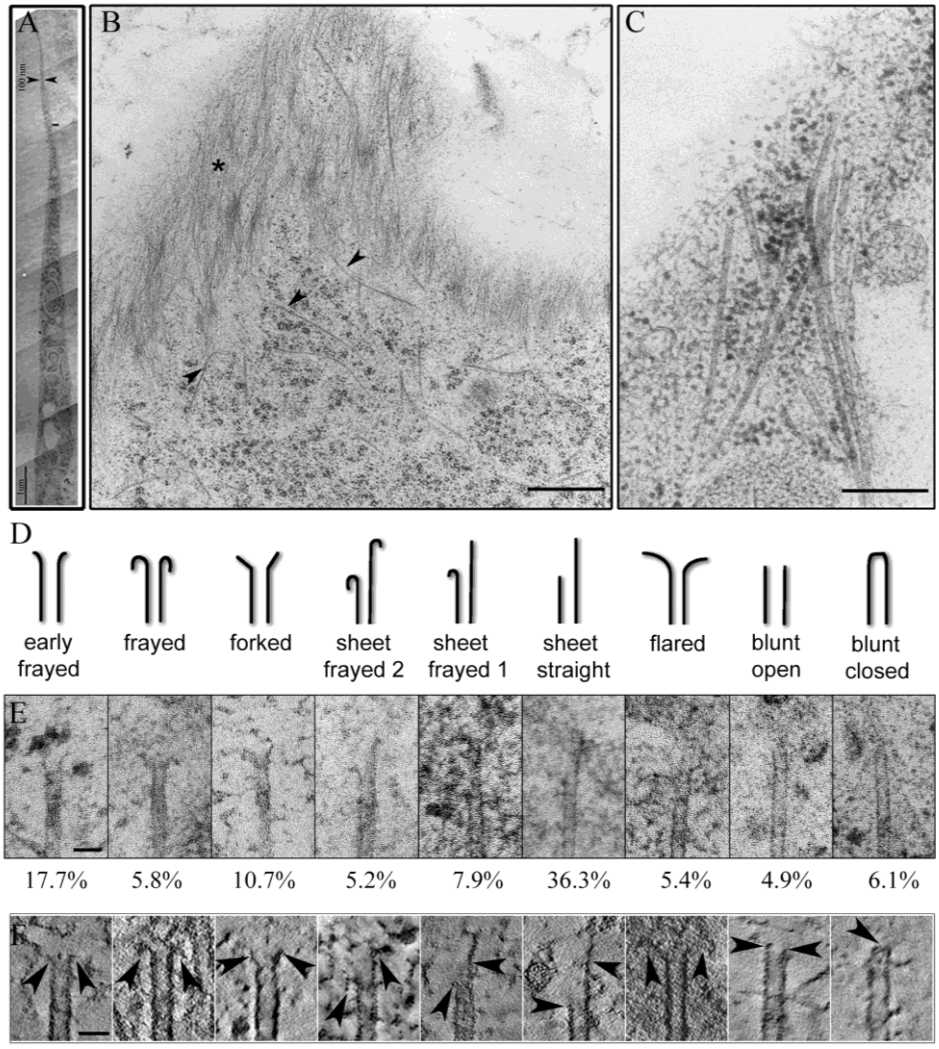


**Figure 1**. Nine distinct plus-end conformations in the periphery of the 3T3 cells. (A) Ten stitched micrographs showing the side view (section perpendicular to cell attachment plane) of the periphery of a sectioned cryo-fixed, freeze-substituted and flat embedded 3T3 cell. The cells become as thin as 80nm at the cell periphery (thickness indicated by the two arrows is 100nm). Bar 1µm. (B) Periphery of a 3T3 cell, sectioned parallel to its attachment plane, with MTs running towards the cell membrane (arrows) and cortical actin filaments (asterisk). Bar, 0.5µm. (C) MT plus-ends in proximity of the cell border. Bar, 0.3µm. (D) Cartoon of MT plus-ends conformations found in the periphery of the 3T3 cells with class annotation below each image. From left to right: *early-frayed, frayed, forked, sheet-frayed 2, sheet-frayed 1, sheet-straight, flared, blunt-open* and *blunt-closed* conformation. (E) Electron micrographs of the nine plus-end conformations corresponding to the cartoons in D. The percentages underneath the micrographs stand for the frequency of a particular plus-end conformation in control 3T3 cells. Bar, 50nm. (F) 5 nm thick tomographical slices of plus-end conformations shown in the same order as in D and E. Arrows point to the plus-end tips. Bar, 50nm.

(n = 29, with mean 105 ± 62nm), i.e. approximately 6-40 tubulin subunits. This is in the same range as the length reported by Austin *et al* for *sheet* ends in plant cells (50-300nm; Austin *et al.,* 2005).
The *sheet-frayed 1* conformation is a combination of *sheet-straight* and *sheet-frayed 2* ends as it has both a straight extension and a curved part. The *flared* end has long, smoothly curving protofilaments extending away from the MT axis. Similar to *forked* ends, *flared* ends have a funnel-like shape and sometimes it was difficult to distinguish between *forked* and *flared* ends. However, the straight protofilaments typical for *forked* are not present in *flared* ends. *Flared* ends have been observed previously by others (Mandelkow *et al*., 1991, first image on the left in Figure 2c).
Finally, we classified *blunt-open* and *blunt-closed* ends. In the first the protofilaments are straight and terminate more or less simultaneously. In the *blunt-closed* end we observe a rounded, cap-like structure at the very tip of the MT.
Next we analyzed the frequency of each plus-end conformation in the cell periphery, extending maximally 5 µm from the cell membrane towards the interior (Figure 1E, frequencies are shown in percentage below the different panels). Out of a total of 164 plus-ends, most ends (36.3 percent) were found to exhibit a *sheet-straight* conformation. The second-largest fraction is formed by the *early-frayed* ends (~18 percent). *Forked* ends (~11 percent) and *sheet-frayed 1* ends (~8 percent) are present in intermediate amounts, whereas the *frayed* ends (~6 percent), *sheet-frayed 2* ends (~5%), *flared* ends (~5%) *blunt-open* and *blunt-closed* ends (together ~11 percent) are present in lower numbers (Figure 1E).

***Half of the plus-ends in the 3T3 periphery are decorated by EB1***

The growing plus-ends of MTs are easily distinguished in fluorescence microscopy with antibodies against plus-end binding proteins (+TIPs), such as EB1 (Stepanova *et al.,* 2003). We estimated the fraction of plus-ends of growing MTs in the periphery of the 3T3 cells by immuno-labeling MTs and their growing plus-ends with antibodies against tubulin and EB1 respectively (Figure 2). We ensured that the results obtained by fluorescence microscopy could be correlated with our EM data (see *Material and Methods*). We analyzed the total amount of MT plus-ends and plus-ends of growing MTs in an area that was maximally 5 µm from the cell membrane. We analyzed six representative cells and found that the mean percentage of EB1-labeled MT plus-ends was 53.7 ± 19.5 % (in total 686 MT plus-ends counted, ±115 per cell), indicating that half of the MTs in the periphery of the cell were growing.

***Nocodazole affects the distribution of plus-end conformations***

In order to correlate the MT plus-end conformation to the actual dynamic state of a MT, we shifted the balance of dynamic instability towards shrinkage by exposing cells to nocodazole. Nocodazole binds free GTP-tubulin, which can no longer be incorporated into MTs. Thus, nocodazole inhibits MT growth and therefore induces MT dissociation. This MT dissociation is a first-order reaction since it is independent of the concentration of free tubulin, as nocodazole prevents the latter from re-associating. After 130 seconds of nocodazole treatment, MTs were still present in the periphery of the cells, as observed with LM of fluorescently labeled MTs (Figure S1, Supplemental data).

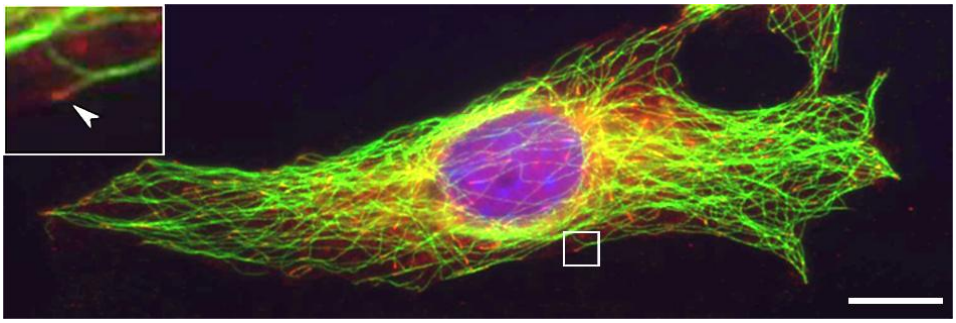

**Figure 2**. Fluorescent microscopy image of a cryo-vitrified, freeze-substituted and subsequently fluorescently stained 3T3 cell with MTs in green, EB1 in red and nucleus in blue. MTs often extend from the area around nucleus towards the cell border. MT plus-ends labeled with EB1 are in the growth phase (arrowhead in the upper left panel). Counting the MT plus-ends (total) and EB1-labeled plus-ends, a fraction of growing plus-ends was assessed. Bar, 10µm.

Next we examined the periphery of nocodazole-treated cells by EM. We analyzed in total 451 MT plus-ends in nocodazole-treated cells. We observed that the fractions of the various conformations of plus-ends altered as a function of the duration of exposure to nocodazole (Figure 3A-H, measured values given by squares). The adjunct values are given in Table 1 (Supplemental data).

Nocodazole clearly causes a significant shift towards the generation of *frayed* ends, *i.e.* MT ends with ram's horns. After 130 seconds of exposure ~80% of the plus-ends exhibited a *frayed* conformation (Figure 3A). We observed an increase of *sheet-frayed 1* upon 15 seconds and 40 seconds of nocodazole-exposure, followed by a decrease as the treatment continued (Figure 3B). A similar trend was observed for *sheet-frayed 2* ends, yet here the increase peaked at a later time point, i.e. after 70 seconds of nocodazole-exposure (Figure 3C). *Flared* end frequency increased after 15 and 40 seconds of nocodazole-exposure, to go down to the basic levels after 70 seconds of exposure (Figure 3D). By contrast, the frequency of *early-frayed* ends decreased from 17% to 9% in the first 15 seconds of exposure to nocodazole to remain relatively constant after prolonged exposure (Figure 3E). Nocodazole treatment also affected the frequencies of *sheet-straight* end and *forked* ends, which dropped from 36 % to 0% for the *sheet-straight* and from 11% to 4 % for the *forked* ends after nocodazole-exposure for 130 seconds (Figure 3F and Figure 3G, respectively). The *blunt-open* frequency also decreased upon exposure to nocodazole (Figure 3H). Finally, *blunt-closed* ends disappeared already after 15 seconds of nocodazole exposure, suggesting that if the *blunt-closed* form represents a MT minus-end, nocodazole also influences the minus-end cap.

In order to characterize the kinetics of MT depolymerization, we determined the set of rate equations that best explained our observed data. We fitted a set of 8 differential equations with 56 unknown rate constants to the kinetic experimental data (lines in the

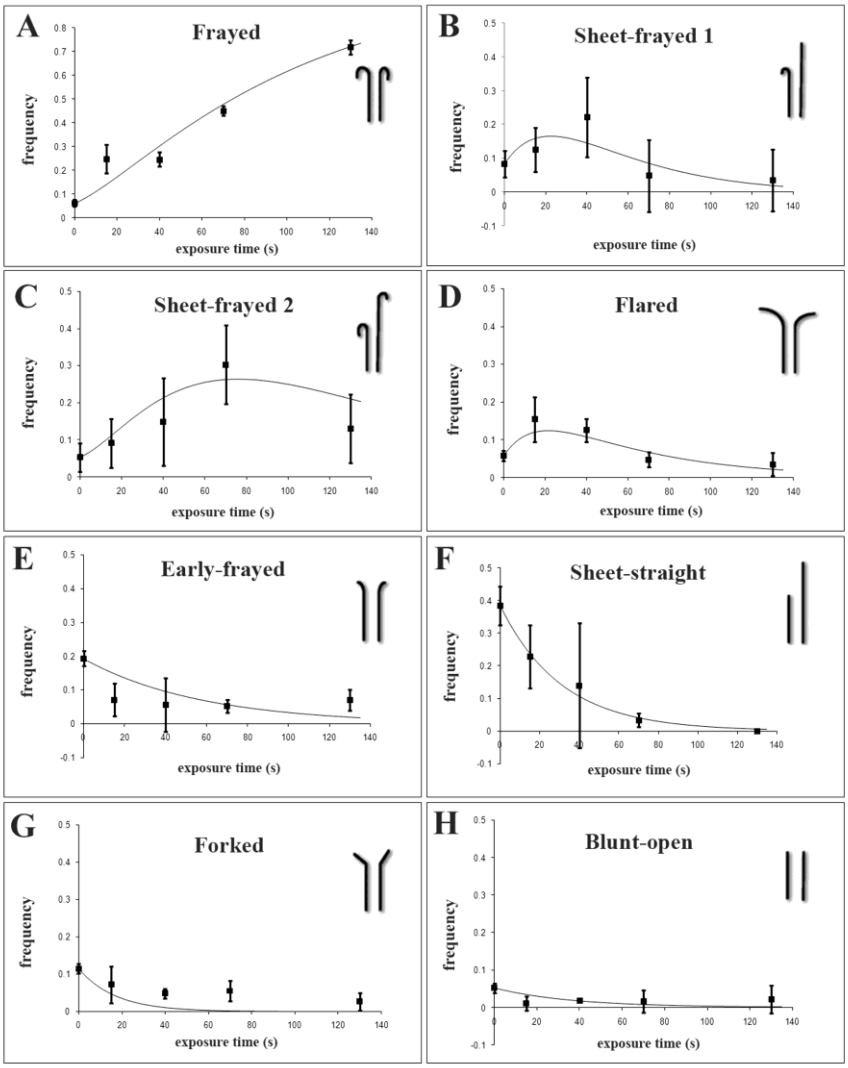


**Figure 3**. Nocodazole alters the ratios of plus-end conformations in 3T3 cells. 3T3 cells were exposed to 10µM nocodazole for 0, 15, 40, 70 and 130 seconds respectively. We scored various plus-ends conformations in the area 0-5 µm from the cell border into the cell center for each time point. The measured values are represented by squares. We fitted the kinetic data (black curves in the graphs) to a set of linear differential equations by minimizing the chi-squared value between the predicted and observed frequencies. Nocodazole clearly caused a significant shift towards generation of *frayed* ends (A) and loss of *sheet-straight* ends (F). The frequency of the *sheet-frayed 1* and *sheet-frayed 2* ends increased during the first 40 and 70 seconds respectively, to decrease again after prolonged exposure to nocodazole (B, C). The same trend was observed for *flared* ends, however the peak frequency for these ends was reached at t =15 seconds (D). Nocodazole induced a decrease of frequency of the *early-frayed* (E), *forked* (G) and *open-blunt* ends (H). Note the larger scale used in panel (A). For the numerical representation of these data see Table 1 (Supplemental material).

graphs shown in Figure 3A-H). Each of the 8 differential equations had the following form:

$$\delta[M_a] / \delta t = k_{ba}[M_b] + k_{ca}[M_c] + k_{da}[M_d] + k_{ea}[M_e] + k_{fa}[M_f] + k_{ga}[M_g] + k_{ha}[M_h]$$

$$- (k_{ab} + k_{ac} + k_{ad} + k_{ae} + k_{af} + k_{ag} + k_{ah})[M_a]$$

where $k_{xy}$ is the rate constant of the transition of $M_x$ into $M_y$ and $[M_a]$ to $[M_h]$ are the observed frequencies at a given time point of each of the types of microtubule ends (either *early-frayed, frayed*, *forked*, *sheet-frayed 1*, *sheet-frayed 2, sheet-straight*, *flared* and *open blunt*). We did not include the *blunt-closed* ends in our analysis since previous studies suggested this conformation to be a MT minus-end (O'Toole *et al.,* 2003) and since this plus-end conformation was not observed in the presence of nocodazole.

Subsequently, the fit – as defined by the $\chi^2$ statistic – between the calculated kinetic model and the observed, experimental kinetic data, was optimized using the standard simplex minimization procedure implemented in the GNU Scientific Library (GSL). We implemented an algorithm based on simplex minimization, that allows all rate constants to vary independently, and that converges on a combination of rate constants that correspond to a maximum of the $\chi^2$ statistic. In order not to bias the result to any pre-supposed mechanism, we initially allowed all interchanges between all the different plus-end conformations, even very unlikely transitions (e.g. *sheet-frayed 1* into *sheet-straight*). In order not to bias the result to the initial values assigned to the rate constants at the start of the fitting procedure, we repeated the analysis, starting with many different (combinations of) initial rate constants. In all cases, most of the rate constants converged to zero within a few cycles of minimization, indicating that the corresponding transitions were forbidden by any kinetic model. When rate constants vanished in this fashion, we fixed them to zero, effectively prohibiting the corresponding transition in subsequent refinement steps. Fitting procedures starting from many different combinations of rate constants all converged to just a few potential models and from these models we selected the one with the highest similarity between interchanging plus-ends. The most probable model is a compromise between the precision of the fit and the number of kinetic rate constants that are needed to explain the data. The $\chi^2$ statistic allowed us to calculate the kinetic model with the highest probability (*i.e.* the best fit with the least number of kinetic rate constants). For the forked plus-end, this procedure resulted in an apparently suboptimal fit, with most data points above the curve. However, as a result of this particular suboptimal fit, the other kinetic curves could be fitted much more accurately. The most likely kinetic model had 7 free parameters (the 7 rate constants we report here), 40 observed restraints with standard deviations and its $\chi^2$ statistic was 15.11, indicating a Q-value (or probability that the result was not obtained by chance fluctuations) of 0.997. This kinetic model conformed in general terms to existing models of microtubule depolymerization.

According to our kinetic analysis three types of transition can occur upon nocodazole exposure (Figure 4). In the first (Figure 4, vertically arranged set of transition reactions), the *sheet-straight* end transforms into the *sheet-frayed 1* end (rate constant is 0.03 $s^{-1}$), and this end transforms into the s*heet-frayed 2* end (rate constant is 0.04 $s^{-1}$). The

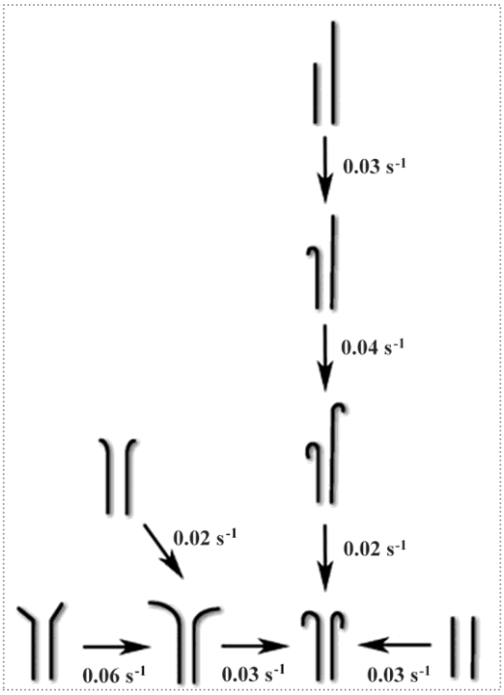


**Figure 4**. Transformation path model for *in vivo* microtubule plus-end conformations. Arrows stand for transitions between the dynamic plus-end states estimated by kinetic analysis after exposing cells to nocodazole. Calculated rate constants are given for each transition. According to our analysis, upon nocodazole treatment a plus-end with a *sheet-straight* conformation transforms into a *sheet-frayed 1*, which upon prolonged nocodazole-exposure transforms into *sheet-frayed 2*, switching eventually into a *frayed* end (vertical path). Another path starts with a *forked* end which transits into a *frayed* end via *flared* conformation (horizontal path). Similarly to a *forked* conformation, *early-frayed* transits into a *frayed* end via *flared* conformation. A *blunt-open* end directly transits into a *frayed* end upon nocodazole-induced disassembly.

*sheet-frayed 2* end subsequently transforms into a *frayed* end (rate constant is 0.02 $s^{-1}$). A second transition path leads from the *forked* and *early-frayed* end towards the *frayed* end (Figure 4, left hand set of reactions). Here, the *forked* and *early-frayed* ends transform into a *flared* end (rate constant are 0.06 $s^{-1}$ and 0.02 $s^{-1}$, respectively) and a *flared* end subsequently converts into a *frayed* end (rate constant is 0.03 $s^{-1}$). Finally, a *blunt-open* end can also transform into a *frayed* end (rate constant is 0.03 $s^{-1}$) without any intermediate form (Figure 4, right hand reaction). The kinetic analysis suggests that *sheet-straight*, *blunt-open*, and (at least a fraction) of *forked* and *early-frayed* ends is likely to represent the growing states of MT plus-ends while the *frayed* ends are confirmed to represent the shrinking ends. *Flared*, *sheet-frayed 1* and *2* might represent transition states originating from growing MT plus-ends that have undergone catastrophe.

***The cell periphery affects plus-end conformations***

In the cell interior MTs grow (or shrink) persistently, whereas close to the membrane an oscillatory behavior is observed, with individual MTs frequently switching between phases of growth, pause and shrinkage (Komarova *et al.,* 2002)**.** According to our data at dynamic equilibrium, 34% of the population of the MTs in the searched area (0-5 microns from the cell periphery) was associated with shrinking ends (*frayed, early-frayed, flared* and *sheet-frayed 2* together) while 52% of MTs was associated with stable and/or growing ends (*forked*, *blunt-open* and *sheet-straight* together). The latter number is in close agreement with our immunofluorescence data using antibodies against EB1. Thus,

using EM methods we detect 1.5 times more conformations associated with growing plus-ends than shrinking ones.

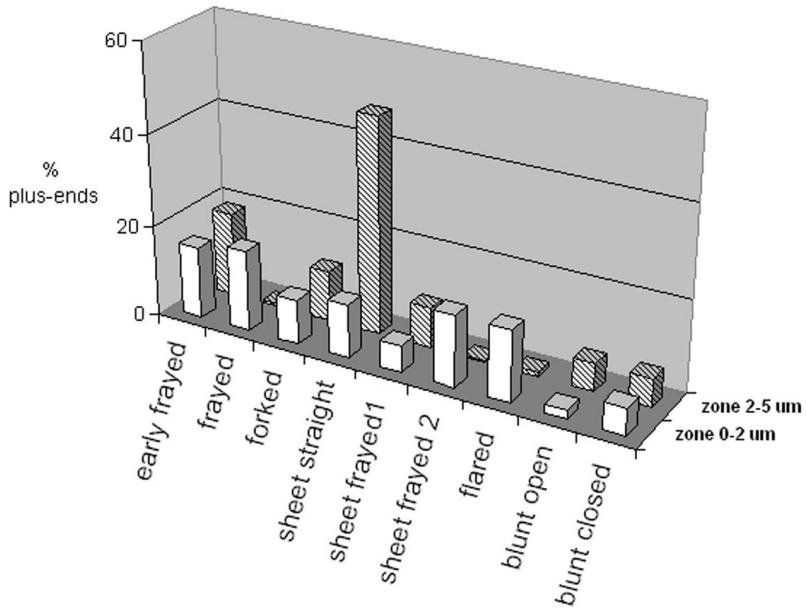


**Figure 5**. Effect of proximity of the cell border on the distribution of the plus-end conformations in the cell periphery. Periphery of the 3T3 cell was divided in two zones from the cell border towards the cell interior, zone 0-2 µm and 2-5 µm from the cell border (with cell border at the position 0 µm). In the zone 0-2 µm and in the zone 2-5 µm respectively 51 and 113 MT plus-ends were counted. The values were normalized for total number MTs per zone. In the zone 0-2 µm (white bars) *(early) frayed, sheet-frayed 2* and *flared* plus-ends were most prominent (each about 16-17%). Except for *early-frayed* end, the frequency of these plus-ends decreased with the increasing distance from the cell border (zone 2-5 µm, striped bars). *Sheet-straight* end and *blunt-open* end were less frequent in zone 0-2 µm (respectively 12% and 2%), nevertheless, in zone 2-5µm these plus-end conformations were much more prominent (respectively 47% and 6%). The *early-frayed*, *forked, sheet-frayed 1* and *blunt-closed* conformations were evenly distributed in the two zones. The percentages and absolute numbers are given in Table 2 (Table 2, Supplemental data).

In order to test whether the cell periphery affects MT plus-end conformation, we examined if there is a correlation between plus-end conformation and spatial distribution within the peripheral area of the cell. In a zone that was 0-2 µm from the cell membrane we measured the conformation of 51 MT plus-ends and in a zone of 2-5 µm from the membrane we measured 113 MT plus-ends. Figure 5 shows the distribution of plus-ends per class and per zone. The adjunct values are given in Table 2 (Supplemental data). The frequency of *frayed*, *sheet-frayed 2* and *flared* ends was higher in the zone closest to the membrane (each about 15-17% versus 0.5-1 %, respectively). By contrast, the *sheet-straight* and *blunt-open* ends were much less frequent near the cell edge (12% and 2% respectively in 0- 2 µm zone, versus 47 % and 6% in 2-5 µm zone). *Early-frayed, forked, sheet-frayed 1* and *blunt-closed* ends were more or less evenly distributed. In the 0-2 µm zone, 45% of the plus-ends have conformations associated with shrinkage

(*frayed*, *sheet-frayed 2* and *flared* ends), while the typical growth-associated conformations (*forked, sheet-straight* and *blunt open)* make ~24%. Furthermore, in the zone 2-5 µm the growth-associated conformations are dominant over the shrinkage-associated conformations (Figure 5). Combined the data show that the features present in the cell periphery do affect MT plus-end conformation.

## Discussion

We observed nine predominant types of in MT plus-end conformations at the periphery of interphase 3T3s, which we have categorized as *early-frayed, frayed*, *forked*, *sheet-frayed 1*, *sheet-frayed 2, sheet-straight*, *flared, blunt-open* and *blunt-closed*. We distinguished these types on the basis of their appearance and their kinetic behavior. Most of these plus-end conformations have previously been observed on *in vitro* assembled MTs and *in situ* kMTs, although the nomenclature of plus-end conformations used in different reports is not completely consistent. The *sheet-frayed 2* form has, to our knowledge, not been reported until now. Our data indicate that nocodazole causes an increase in *frayed* plus-end frequency. This finding is in agreement with *in vitro* studies (Mandelkow and Mandelkow, 1985; Mandelkow *et al*., 1991; Chrétien *et al*., 1995; Müller-Reichert *et al*., 1998; Arnal *et al*., 2000) and *in situ* studies on kMTs (VandenBeldt *et al*., 2006) and indicates that the shrinking MT plus-end adopts the *frayed* conformation. We conclude that interphase MTs at the cell periphery of 3T3 fibroblasts resemble *in vitro* assembled and kMTs in many aspects and can be used to understand and interpret the different dynamic states of a MT *in situ.*

Loss of *sheet-straight* plus-ends upon introduction of nocodazole suggests that these represent the fraction of growing plus-ends (Figure 3F). *Sheet-straight* ends were indeed previously found to be associated with growth in *in vitro* cryo-EM studies (Chrétien *et al.,* 1995). *Sheet-frayed 1* and *sheet-frayed 2* end frequencies first increased and then decreased upon prolonged nocodazole-exposure. The increase could be due to disappearance of the *sheet-straight* fraction. At the point the *sheet-frayed 1* started to decrease, *sheet-frayed 2* increased, reaching a peak value at 70 seconds of exposure (Figure 3B, C). This indicates that the *sheet-frayed 2* end is the stage following the *sheet-frayed 1* towards the *frayed* end generation (Figure 4).

If we consider the morphology of the *sheet-frayed 1* ends, we both find features of MT growth (sheet, GTP-tubulin) and shrinkage (frayed, GDP-tubulin) in this structure. This was also indicated by others (VanBuren *et al*., 2005), who suggested that these plus-ends, having 7 of 13 protofilaments GTP-capped, could have growing and shrinking protofilaments at the same time. Once the straight end starts to curve, the extended sheet would shrink more rapidly than the protofilaments at the base of the MT tip, possibly due to the lack of the lateral contacts of the outer layer of protofilaments in the extension. We propose here that the *sheet-frayed 1* and *2* conformations are the transition states originating from the *sheet-straight* rather than from the *blunt-open* conformation. Our kinetic analysis is supported by the findings of VanBuren *et al.* (VanBuren *et al.,* 2005) who suggested that a *sheet-straight* end is more likely to collapse/shrink than a *blunt-open* end. A striking finding from our kinetic analysis is that in a *sheet-straight* plus-end the protofilaments on the “short” side of the plus-end are the first to curve out and depolymerize. Only then do protofilaments on the “extended” side of the plus-end start to curve out. An attractive interpretation is that +TIPs are

preferentially bound to the extended side of the MT. By maintaining the extended sheet in its straight conformation MTs are “induced” to grow, even when the “short” side of the MT temporarily curves out.

*Early-frayed*, *forked* and *blunt-open* ends disappear gradually upon nocodazole-exposure, while the *flared* end frequency first increases and then decreases during the nocodazole treatment. It is rather difficult to directly deduce from the measured data in Figure 3 which transition paths these ends follow, except that they all eventually transform into the *frayed* end. However, by means of kinetic analysis we were able to calculate the rates of probable transformations (Figure 4). Our kinetic analysis suggests that the *early-frayed* and *forked* ends both transform into *flared* ends, which in turn transform into *frayed* ends. In *flared* ends the lateral interactions between curving protofilaments are clearly lost, giving rise to further disassembly. In our model a *blunt-open* end converts into a *frayed* end. *Blunt-open* and *forked* ends both have straight protofilaments, a feature associated with the presence of the GTP-state of tubulin and therefore the growing state of MT (Howard *et al*., 1986; Wang and Nogales, 2005; Schek *et al*., 2007). Given this, in combination with the effect of nocodazole on these conformations, the *forked* and *blunt-open* ends could possibly represent growing/stable conformations. For *forked* ends this was recently suggested by others (Höög *et al.*, 2007). Note that in the latter study the forked end was named and interpreted as *“flared”*.

Interestingly, the *early-frayed* end has slightly curved protofilaments at the tip. Still it disappears upon prolonged nocodazole treatment (Figure 3E), which indicates that it might represent a stable/growing phase. An explanation might be found in the structural-cap model, described by Janosi *et al* in which the protofilaments at the tip of the *blunt-open* end slightly curve as a result of ‘relaxation’ of the mechanically stressed, though elastic, tube (Janosi *et al.,* 2002). These ends were suggested to be (meta)stable, pausing ends, which could transition into shrinkage or growth, depending on the circumstances. It is possible that, at least for some fraction of the found *early-frayed* ends, this is true. How these ends are generated is not clear to us, as we do not find a transition path between e.g. *blunt-open* and *early-frayed* ends.

Using LM we found approximately 54% of the plus-ends to be growing (i.e. carrying the protein EB1). This value is in the same range as the sum of the fractions of *sheet-straight* (37%), *forked* (11%) and *blunt-open* (5%) ends found in our EM experiments (Figure 1E). These ends might therefore possibly contain structures recognized by EB1. It has been previously suggested that +TIPs might recognize the lumen side of the sheet (Nogales and Wang, 2006). Given the size of GFP-tagged +TIP comets (Perez *et al*., 1999; Mimori-Kiyosue *et al*., 2000), this would mean that the lumen of the MT would have to be accessible over a range of a few microns. However, we found the maximal sheet length *in situ* to be 320 nm, which is in the same range as the sheet length reported by others (Austin *et al.*, 2005). It was found that +TIPs exchange very rapidly on MT plus-ends *in vivo* and that this exchange is governed by cytoplasmic diffusion (Dragestein *et al*., 2008). Together these observations make it unlikely that +TIPs bind the lumen side of MTs.

In close proximity of the cell border (zone <2µm, Figure 5) *sheet-frayed 2*, *flared* and *(early) frayed* ends predominate over *blunt*, *forked, sheet-straight* and *sheet-frayed 1* ends. Plus-ends associated with shrinkage (i.e. *frayed, flared* and *sheet-frayed 2*) are rather scarce in zone 2-5 µm and plus-ends associated with MT growth (*sheet-straight,*

*blunt-open*) are not as frequent in the area in close proximity of the cell border (zone <2µm), as they are in the area further away from it. This indicates that the dynamic status of a plus-end is influenced by features present in the periphery.

The finding that the ratio of "growth-like" to "shrinkage-like" conformations is approximately 1.5:1 instead of 2.5:1 (which would be expected at steady state; Komarova *et al.*, 2002; Grigoriev *et al.*, 2006), suggest that a fraction of MTs with a "shrinking" type of conformation might actually not be shrinking, but is instead captured and embedded near the cell membrane by anchoring factors. This, was recently also suggested for the *frayed* plus-ends in kMTs (VandenBeldt *et al.*, 2006). Such stabilization could, for example, be achieved by anchoring of the MT plus-end in the cortical actin meshwork. Proteins that are thought to play a role in MT capture mechanisms in the cell periphery include the CLASPs, IQGAP1 and ACF7 (Akhmanova *et al*., 2001; Fukata *et al.*, 2002; Kodama *et al*., 2003). With the data reported here, it is not possible to distinguish such stabilized *frayed* plus-ends from the shrinking ones. Nevertheless, the capture of *frayed* plus-ends would explain the shifted ratio of shrinking/growing ends we found in the periphery of untreated 3T3s.

In conclusion, we have identified nine interchangeable conformations of MT plus-ends which are present in the cell periphery of interphase mammalian cells. By combining ET, EM and LM techniques we linked MT plus-end conformation to dynamic state. We propose a kinetic model of plus-end transitions from the growing towards the shrinking conformation. Our data indicate that shrinking plus-ends might be stabilized by cellular factors associated with the cellular periphery.

## Acknowledgements

We would like to thank Raimond Ravelli and Roman Koning for helpful discussions. This work was supported by the Netherlands Organization for Scientific Research (NWO) and the Dutch Ministry of Economic Affairs (BSIK).

## References


Akhmanova, A.*, et al.* (2001). Clasps are CLIP-115 and -170 associating proteins involved in the regional regulation of microtubule dynamics in motile fibroblasts. Cell. *104(6),* 923-35.

Arnal, I., Karsenti, E., and Hyman, A.A. (2000). Structural transitions at microtubule ends correlate with their dynamic properties in Xenopus egg extracts. J. Cell. Biol. *149(4)*:767-774.

Austin, JR 2nd., Segui-Simarro, J.M., and Staehelin, L.A. (2005). Quantitative analysis of changes in spatial distribution and plus-end geometry of microtubules involved in plant-cell cytokinesis. J. Cell. Sci. *118(Pt 17)*, 3895-3903.

Caplow, M., and Reid, R. (1985). Directed elongation model for microtubule GTP hydrolysis. Proc. Natl .Acad. Sci. U S A. *82(10),* 3267-3271.

Caplow, M. (1992). Microtubule dynamics. Curr. Opin. Cell. Biol. *4(1)*, 58-65.

Caplow, M., Ruhlen, R.L.,and Shanks, J. (1994b).The free energy for hydrolysis of a microtubule-bound nucleotide triphosphate is near zero: all of the free energy for hydrolysis is stored in the microtubule lattice. J. Cell. Biol. *127(3)*, 779-88.

Chrétien, D., Fuller, S.D., and Karsenti, E. (1995). Structure of growing microtubule ends: two-dimensional sheets close into tubes at variable rates. J. Cell. Biol. *129(5)*, 1311-1328.

Dragestein, K.A., van Cappellen, W.A., van Haren, J., Tsibidis, G.D., Akhmanova, A., Knoch, T.A., Grosveld, F., Galjart, N. (2008). Dynamic behavior of GFP-CLIP-170 reveals fast protein turnover on microtubule plus ends. J Cell Biol. *180(4),* 729-37.

Fukata, M., Watanabe, T., Noritake, J., Nakagawa, M., Yamaga, M., Kuroda, S, Matsuura, Y, Iwamatsu, A., Perez, F., and Kaibuchi, K. (2002). Rac1 and Cdc42 capture microtubules through IQGAP1 and CLIP-170. Cell. *109(7),*873-885.

Grigoriev, I., Borisy, G., and Vorobjev, I. (2006). Regulation of microtubule dynamics in 3T3 fibroblasts by Rho family GTPases. Cell. Motil. Cytoskeleton. *63(1)*, 29-40.

Höög, J., Schwartz, C., Noon, A., O'Toole, E., Mastronarde, D., McIntosh, J., and Antony, C. (2007). Organization of Interphase Microtubules in Fission Yeast Analyzed by Electron Tomography. Developmental Cell. *12,* 349-361.

Howard, W.D, and Timasheff, S.N. (1986). GDP state of tubulin: stabilization of double rings. Biochemistry. *25(25)*, 8292-8300.

Janosi, I.M., Chrétien, D., and Flyvbjerg, H. (2002). Structural microtubule cap: stability, catastrophe, rescue, and third state. Biophys. J. *83(3)*, 1317-1330.

Kerssemakers, J.W, Munteanu, E.L., Laan, L., Noetzel, T.L., Janson, M.E., and Dogterom, M. (2006). Assembly dynamics of microtubules at molecular resolution. Nature. *442(7103)*,709-712.

Kodama, A., Karakesisoglou, I., Wong, E., Vaezi, A., Fuchs, E. (2003). ACF7: an essential integrator of microtubule dynamics. Cell. *115(3),* 343-354.

Komarova, Y.A., Akhmanova, A.S., Kojima, S., Galjart, N., and Borisy, G.G. (2002) Cytoplasmic linker proteins promote microtubule rescue in vivo. J. Cell. Biol. *159(4)*, 589-99.

Kovacs, P., and Csaba, G. (2005). Effect of drugs affecting microtubular assembly on microtubules, phospholipid synthesis and physiological indices (signalling, growth, motility and phagocytosis) in Tetrahymena pyriformis. Cell. Biochem. Funct. *24(5),* 419-429.

Krebs, A., Goldie, K.N., and Hoenger, A.(2005). Structural rearrangements in tubulin following microtubule formation. EMBO Rep. *6(3)*, 227-232.

Lansbergen, G. and Akhmanova, A. (2006). Microtubule plus end: a hub of cellular activities. Traffic. *7(5),* 499-507.

Lieuvin, A., Labbe, J.C., Doree, M., and Job, D. (1994). Intrinsic microtubule stability in

interphase cells. J. Cell. Biol. *124(6)*, 985-996.

Maiato, H., Hergert, P.J., Moutinho-Pereira, S., Dong, Y., VandenBeldt, K.J., Rieder, C.L., and McEwen, BF. (2006). The ultrastructure of the kinetochore and kinetochore fiber in Drosophila somatic cells. Chromosoma. *115(6),* 469-480.

Mandelkow, E. and Mandelkow, E.R. (1985) . Unstained microtubules studied by cryo-electron microscopy. Substructure, supertwist and disassembly. J. Mol. Biol. *181(1)*,123-135.

Mandelkow, E.M., Mandelkow, E. and Milligan, R.A. (1991). Microtubule dynamics and microtubule caps: a time-resolved cryo-electron microscopy study. J. Cell. Biol. *114(5)*, 977-991.

Mimori-Kiyosue, Y., Shiina, N. and Tsukita, S. (2000). The dynamic behavior of the APC-binding protein EB1 on the distal ends of microtubules. Curr Biol. *10(14)*, 865-868.

Mitchison, T., and Kirschner, M. (1984). Microtubule assembly nucleated by isolated centrosomes. Nature. *312(5991)*, 232-237.

Mitchison, T.J., (1993). Localization of an exchangeable GTP binding site at the plus end of microtubules. Science. *261*, 1044-7.

Nogales, E., and Wang, H.W. (2006). Structural intermediates in microtubule assembly and disassembly: how and why? Curr Opin Cell Biol. *18(2)*, 179-184.

O'Toole, E.T., McDonald, K.L., Mantler, J., McIntosh, J.R., Hyman, A.A., and Muller-Reichert, T. (2003). Morphologically distinct microtubule ends in the mitotic centrosome of Caenorhabditis elegans. J Cell Biol. *163(3),* 451-456.

Perez, F., Diamantopoulos, G.S., Stalder, R., and Kreis, T.E. (1999). CLIP-170 highlights growing microtubule ends in vivo. Cell. *96(4)*, 517-527.

Ravelli, R.B.G, Gigant, B., Curmi, P.A., Jourdain, I., Lachkar, S., Sobel, A. and Knossow, M. (2004). Insight into tubulin regulation from a complex with colchicine and a stathmin-like domain**.** Nature**.** *428*, 198-202.

Ress, D., Harlow, M.L., Schwarz, M., Marshall, R.M., and McMahan, U.J. (1999). Automatic acquisition of fiducial markers and alignment of images in tilt series for electron tomography.J Electron Microsc. *48(3),* 277-287.

Saoudi, Y., Fotedar, R., Abrieu, A., Doree, M., Wehland, J., Margolis, R.L, and Job, D. (1998). Stepwise reconstitution of interphase microtubule dynamics in permeabilized cells and comparison to dynamic mechanisms in intact cells. J Cell Biol. *142(6),* 1519-1532.

Schek, H.T. 3rd, Gardner, M.K., Cheng, J., Odde, D.J., Hunt, A.J. (2008). Microtubule assembly dynamics at the nanoscale. Curr Biol. *17(17),* 1445-1455.

Stepanova, T., Slemmer,J., Hoogenraad, C.C, Lansbergen, G., Dortland, B., De Zeeuw, C.I., Grosveld, F., van Cappellen, G., Akhmanova, A., Galjart, N. (2003). J Neurosci. *23(7*), 2655-2664.

VanBuren, V., Cassimeris, L., and Odde, D.J. (2005). Mechanochemical model of microtubule structure and self-assembly kinetics. Biophys J. *89(5)*, 2911-2926.

VandenBeldt, K.J., Barnard, R.M., Hergert, P.J., Meng, X., Maiato, H., and McEwen, B.F. (2006). Kinetochores use a novel mechanism for coordinating the dynamics of individual microtubules. Curr Biol. *16(12)*, 1217-1223.

Vorobjev, I.A., Alieva, I.B., Grigoriev, I.S., and Borisy, G.G. (2003) Microtubule dynamics in living cells: direct analysis in the internal cytoplasm. Cell Biol Int. *3*, 293-294.

Wang, H.W., and Nogales, E. (2005). Nucleotide-dependent bending flexibility of tubulin regulates microtubule assembly. Nature. *435,* 911-915

## Supplemental material

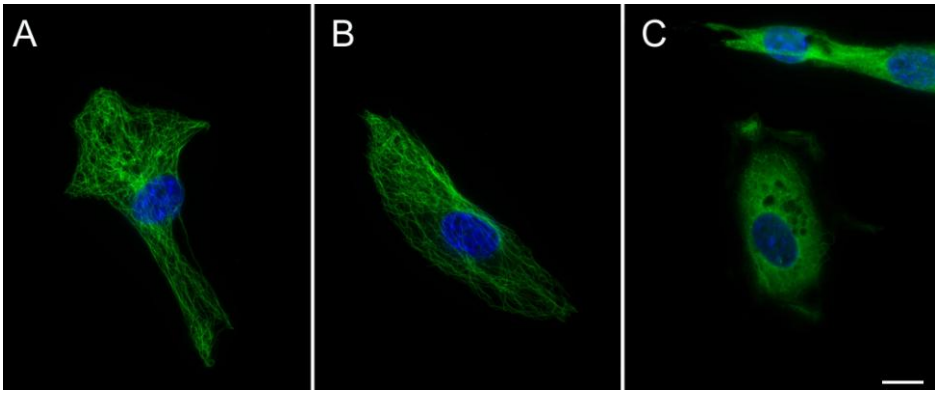


**Figure S1.** Effect of nocodazole exposure on the peripheral MTs in interphase 3T3 cells. 3T3 cells were exposed to 10µM nocodazole for 0 seconds (A), 130 seconds (B) or 30 minutes (C). The MTs are in green and nucleus in blue. 130 seconds long exposure of cells to nocodazole did not seem to cause any major modifications of MTs network in general or retraction of MTs from the cell periphery (B). On the other hand, thirty minute exposure of 3T3s to nocodazole caused almost total loss of MT network (C). Bar, 10µm.

Table 1: Nocodazole affects the frequencies of various plus-ends in the periphery of interphase 3T3 cells in time.

| | **0 seconds** | **15 seconds** | **40 seconds** | **70 seconds** | **130 seconds** |
|---|---|---|---|---|---|
| **Frayed** | 0.062 ± 0.039 | 0.249 ± 0.173 | 0.246 ± 0.063 | 0.451 ± 0.107 | 0.718 ± 0.125 |
| **Sheet-frayed 1** | 0.083 ± 0.021 | 0.126 ± 0.048 | 0.221 ± 0.079 | 0.048 ± 0.019 | 0.035 ± 0.031 |
| **Sheet-frayed 2** | 0.053 ± 0.038 | 0.091 ± 0.066 | 0.148 ± 0.117 | 0.302 ± 0.107 | 0.130 ± 0.092 |
| **Flared** | 0.058 ± 0.014 | 0.154 ± 0.059 | 0.126 ± 0.031 | 0.048 ± 0.019 | 0.035 ± 0.031 |
| **Early-frayed** | 0.193 ± 0.076 | 0.071 ± 0.019 | 0.055 ± 0.038 | 0.052 ± 0.048 | 0.070 ± 0.062 |
| **Sheet-straight** | 0.384 ± 0.0595 | 0.228 ± 0.096 | 0.140 ± 0.192 | 0.034 ± 0.021 | 0.000 ± 0.007 |
| **Forked** | 0.114 ± 0.013 | 0.071 ± 0.050 | 0.048 ± 0.012 | 0.055 ± 0.027 | 0.026 ± 0.023 |
| **Blunt-open** | 0.052 ± 0.013 | 0.011 ± 0.019 | 0.017 ± 0.002 | 0.017 ± 0.030 | 0.022 ± 0.037 |
| ***Total # plus-ends*** | *154* | *100* | *176* | *140* | *35* |

Measured mean plus-end frequencies ± standard deviation (n=3) corresponding to the values represented by squares in Figure 3. In short, 3T3 cells were exposed to 10μM nocodazole for 0, 15, 40, 70 and 130 seconds respectively. Plus-ends conformations were scored in the area 0-5 μm from the cell border into the cell center for each time point. The last row contains absolute number of plus-ends counted per time-point (sum of three experiments).

Table 2. Distribution of nine plus-end conformations over the two zones within the periphery of interphase 3T3 cells.

| | **Early frayed (%)** | **Frayed (%)** | **Forked (%)** | **Sheet straight (%)** | **Sheet frayed 1 (%)** | **Sheet frayed 2 (%)** | **Flared (%)** | **Blunt open (%)** | **Blunt closed (%)** |
|---|---|---|---|---|---|---|---|---|---|
| **Zone 0-2µm** | 15.69 (8/51) | 17.65 (9/51) | 9.80 (5/51) | 11.76 (6/51) | 5.88 (3/51) | 15.69 (8/51) | 15.69 (8/51) | 1.96 (1/51) | 5.88 (3/51) |
| **Zone 2-5µm** | 18.58 (21/113) | 0.44 (0.5/113) | 11.06 (12.5/113) | 47.35 (53.5/113) | 8.85 (10/113) | 0.44 (0.5/113) | 0.88 (1/113) | 6.19 (7/113) | 6.19 (7/113) |

Periphery of a 3T3 cell was divided in two zones from the cell border towards the cell interior, zone 0-2 µm and 2-5 µm from the cell border (with cell border at the position 0 µm). In the zone 0-2 µm and in the zone 2-5 µm respectively 51 and 113 MT plus-ends were counted. The values were normalized for total number MTs per zone. The upper values within a row are percentages, while under this value absolute numbers in the form of (counted plus-ends ends / total ends per zone) is given. Half microtubule means that it could not be classified in only one of the groups; instead it was divided over both groups.